

孙世强, 陈翠华, 赵文皓, 等. 扬子地块西南缘乌斯河富锗闪锌矿矿物标型特征与锗的替代机制[J]. 岩矿测试, 2025, 44(2): 214–229. DOI: [10.15898/j.ykcs.202406210138](https://doi.org/10.15898/j.ykcs.202406210138).

SUN Shiqiang, CHEN Cuihua, ZHAO Wenhao, et al. Mineral Typomorphic Characteristics and Deposit Genesis of Germanium-Enriched Sphalerite from Wusihe in the Southwestern Margin of the Yangtze Block[J]. Rock and Mineral Analysis, 2025, 44(2): 214–229. DOI: [10.15898/j.ykcs.202406210138](https://doi.org/10.15898/j.ykcs.202406210138).

扬子地块西南缘乌斯河富锗闪锌矿矿物标型特征与锗的替代机制

孙世强*, 陈翠华*, 赵文皓, 赖翔, 马天祺, 张海军, 乔梦怡, 宋志娇, 陈宵杰, 辜鹰
(成都理工大学地球与行星科学学院, 四川成都 610059)

摘要: 锗(Ge)是中国优势战略性关键金属之一, 扬子地块西南缘乌斯河铅锌矿床是川—滇—黔成矿带的一个重要富锗铅锌矿床, 其矿床成因仍存在争议, 矿床中闪锌矿的标型特征是否影响Ge的富集程度与替代方式亟待进行解析。为探讨富Ge闪锌矿的标型特征及Ge的替代机制, 本文通过显微镜下观察、显微分光光度计、激光剥蚀电感耦合等离子体质谱(LA-ICP-MS)等分析测试方法对其进行定量研究。结果表明该矿床热液期存在Ⅰ阶段颜色较深闪锌矿和Ⅱ阶段颜色较浅闪锌矿, 视觉反射率均值分别为16.126%、16.187%, 反射色主波段均值分别为474.179nm、474.164nm, 反射色饱和度均值分别为0.048、0.043, Ge含量均值分别为 244.33×10^{-6} 、 43.22×10^{-6} 。通过对实验结果的总结认为, Ge以类质同象的形式存在于闪锌矿中, 且更易在反射色饱和度高的闪锌矿中富集。Ge的替代方式与Cu、Ag有关, 两阶段分别为 $\text{Ge}^{4+} + 2\text{Cu}^+ \leftrightarrow 3\text{Zn}^{2+}$ 、 $\text{Ge}^{4+} + 2(\text{Cu}, \text{Ag})^+ \leftrightarrow 3\text{Zn}^{2+}$ 。富Ge闪锌矿的反射色颜色指数特征指示成矿温度上限为203.0~293.0°C, 微量元素特征指示成矿温度下限为83.3~199.0°C, 矿床成因类型为密西西比河谷型(MVT)铅锌矿床。

关键词: 富锗铅锌矿床; 闪锌矿标形特征; 替代机制; 显微分光光度计; 激光剥蚀电感耦合等离子体质谱; 类质同象; 密西西比河谷型铅锌矿床

要点:

- (1) 显微分光光度计和LA-ICP-MS分析实现了对富Ge闪锌矿的颜色标型和微量元素标型的定量分析, 发现在两阶段闪锌矿中差异性富集Ge。
- (2) 两阶段闪锌矿中Ge以类质同象形式赋存, 替代方式分别为: $2\text{Cu}^+ + \text{Ge}^{4+} \leftrightarrow 3\text{Zn}^{2+}$; $\text{Ge}^{4+} + 2(\text{Cu}, \text{Ag})^+ \leftrightarrow 3\text{Zn}^{2+}$ 。
- (3) Ge更易在反射色饱和度高的闪锌矿中富集, 闪锌矿的矿物标型指示矿床应为中-低温, MVT型。

中图分类号: P578.23; P611

文献标识码: A

Ge以其良好的导热性、导电性、高折射率和低色散性等性质广泛应用于半导体、红外光学、光纤、聚合催化剂和医学等重要领域^[1-2]。Ge作为一种稀散元素, 主要伴生在铅锌矿床和煤矿中, 其中全球近3/4的工业Ge由铅锌矿床中的闪锌矿提供^[3-4]。

矿物标型包括矿物形态、结构、颜色、热电性等物理标型和主微量元素组成、同位素组成等成分标型, 而闪锌矿的矿物标型特征往往能够有效地反映矿床的形成环境及成因类型^[5-6]。因此, 深入研究铅锌矿床中Ge的富集机制和富Ge闪锌矿标型特征, 不仅

收稿日期: 2024-06-21; 修回日期: 2024-08-19; 接受日期: 2024-08-22; 网络出版日期: 2024-10-22

基金项目: 四川省科技厅自然科学基金项目“四川汉源乌斯河铅锌矿床闪锌矿中关键金属锗的富集机制及成因矿物学找矿标志”(2023NSFSC0274)

第一作者: 孙世强, 硕士研究生, 专业方向为矿物学、岩石学、矿床学、矿产普查与勘探研究。

E-mail: 2284726172@qq.com。

通信作者: 陈翠华, 博士, 教授, 主要从事矿床学、矿相学、地球化学研究。E-mail: chencuihua@cdut.edu.cn。

对进一步认识富锗铅锌矿床的成矿规律具有重要意义,也对于Ge资源的勘查和开发具有实际应用价值。

扬子地块周缘是中国最重要的铅锌成矿带之一,也是中国重要的“铅锌型”锗资源基地,区域内发育有川—滇—黔铅锌成矿带、马元—白玉铅锌成矿带、鄂西—湘西—黔东铅锌成矿带等^[7-11]。扬子地块西南缘乌斯河铅锌矿床是川—滇—黔成矿带中重要的铅锌多金属矿床,以其矿石储量丰富(5.4Mt),伴生元素多(如Cd、Ge、Ga等),富Ge等特征被众多专家学者关注,对成矿地质背景^[12]、成矿物质来源^[13-14]、成矿流体特征^[13,15]、岩石地球化学特征^[13-15]、矿床成因^[12-18]有了深入的认识。罗开等^[18]也发现该矿床内不同阶段闪锌矿中差异性富集Ge,闪锌矿的标型特征是否影响Ge的富集仍值得进一步研究。另外,关于乌斯河铅锌矿床的成因仍存在两种不同的认识:喷流—沉积型(SEDEX)矿床^[13]和密西西比河谷型(MVT)矿床^[14,16-18]。

近年来,随着微区原位分析技术快速发展,激光剥蚀电感耦合等离子体质谱(LA-ICP-MS)具有空间分辨率高、分析检出限低和运行成本低等特点广泛应用于岩石矿物多元素微区原位分析^[19-21]。显微分光光度计可以在毫米内获得矿物的反射率、视觉反射率、反射色主波段、反射色饱和度等特征,具有高效、便捷等特点。在地学研究方面,显微分光光度计的应用主要为地层中有机质镜质体反射率的测定,

而对于金属矿物反射率的测定较少。而且较新型的显微分光光度计测试束斑可达微米级别,这与LA-ICP-MS等原位成分测试束斑一致,为矿物的光学特征结合化学特征的分析提供了支持^[6]。因此,本文采用这两种测试手段对富Ge闪锌矿的微量元素组成和反射色颜色指数进行分析,探讨乌斯河铅锌矿床中富Ge闪锌矿的微量元素和颜色标型特征及其指示意义,为后续的勘查找矿工作提供成因矿物学方面的标志证据。

1 研究区地质特征

川—滇—黔成矿带位于扬子地块的西南缘,北接秦岭、松潘—甘孜造山带,南邻三江造山带、华夏板块(图1a)。扬子地块西南缘具有特征的双层结构—基底和盖层,基底由结晶基底与褶皱基底共同组成,盖层由下震旦统的过渡性盖层、上震旦统一上三叠统的海相沉积盖层、上三叠统一第四系的陆相沉积盖层共同组成^[12,18]。在一系列褶皱变形作用下形成了南北向构造与东西向、北西向、北东向构造交织的构造格局。区内岩浆活动频繁,广泛分布峨眉山玄武岩(图1b)。区内矿产丰富,是铅、锌、金、银、锗等金属的重要产出基地,包含会泽、天宝山、大梁子、赤普和乌斯河等超大型、大型铅锌矿床,铅锌储量可达数千万吨^[12],且多伴生稀散元素Ge。

乌斯河铅锌矿床位于大渡河谷北岸(图1c),

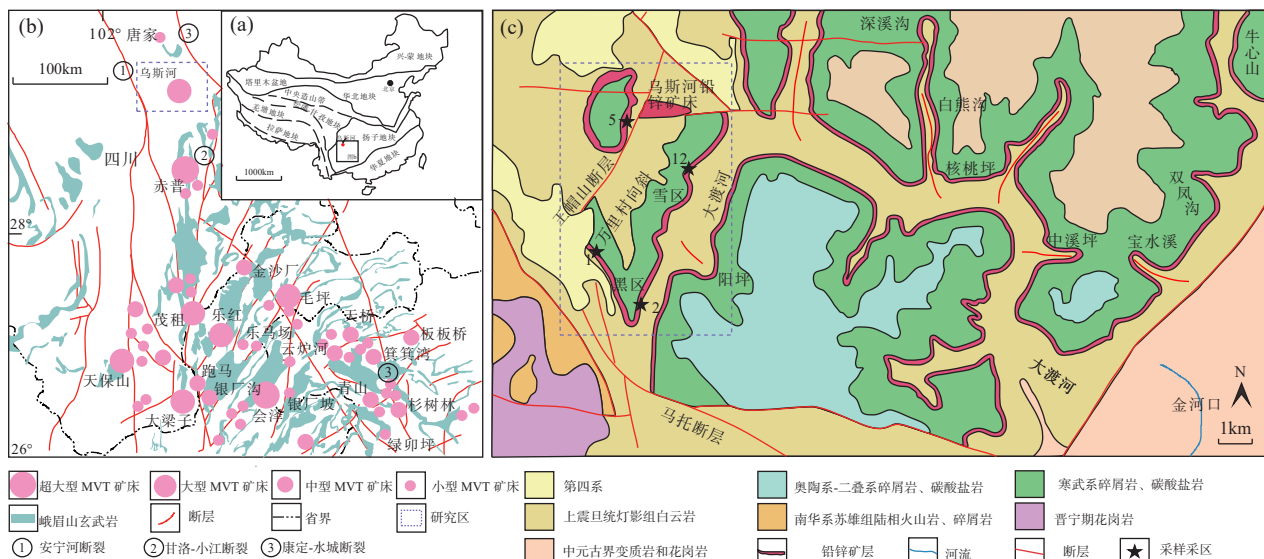


图1 (a) 中国大地构造背景; (b) 扬子地台铅锌矿床分布及研究区位置图(据熊索菲等^[15]); (c) 乌斯河矿床地质图及采样点(据罗开等^[18])

Fig. 1 (a) China's tectonic background; (b) Distribution and location map of lead-zinc deposits in the Yangtze Platform (modified by Xiong, et al.^[15]); (c) Geological map and sampling points of the Wusihhe deposit (modified by Luo, et al.^[18]).

出露震旦系苏雄组、观音崖组、灯影组地层,以及寒武系地层、奥陶系—第二系地层和第四系地层。其中灯影组地层($Z_b d$)主要由白云岩组成,是乌斯河矿床的主要赋矿层位。矿体主要受北西向(NW)马托断层、北西向(NW)王帽山断层以及万里村向斜控制。马托断层位于矿区西南方向,破碎带发育(宽约10~30m),上下盘均为灯影组地层,为逆断层。王帽山断层位于矿区北西方向,破碎带发育(宽约15~30m),上盘震旦系灯影组地层抬升,下盘寒武系至奥陶系地层下降,为逆断层。万里村向斜轴向近南北向,由核部及两翼出露二叠系、志留系、奥陶系、寒武系、震旦系地层,东西两翼岩层倾角不等,属两翼不对称向斜。

乌斯河铅锌矿床是川—滇—黔成矿带内的一个大型铅锌矿床,受构造控制,矿体产出形态主要呈层状、似层状或透镜状,矿化带厚度22.2~32.5m^[18]。矿床的主要金属矿物为闪锌矿、方铅矿、黄铁矿及少量的硫化物矿物,非金属矿物以白云石、石英和方解石为主。

2 实验部分

2.1 样品采集与制备

本文的实验样品主要来自大渡河北岸的乌斯河铅锌矿床,在野外地质调查的基础上,对该地区1采区、2采区、5采区、12采区(图1c)进行系统采样。所取样品涵盖矿床热液成矿期不同阶段,层位为上震旦统灯影组。在此层位矿体主要呈层状,闪锌矿作为矿体主要部分,选取具代表性的矿石样品进行磨制光片和探针片。光片和探针片的磨制在河北省地质测绘院岩矿测试中心完成,光片磨至3.7cm×2.6cm×0.6cm,探针片磨至厚150μm。

经显微镜镜下分析,划分成矿期次,筛选出不同阶段的探针片,分别进行闪锌矿反射色颜色指数分析和闪锌矿微量元素分析。为保证两类原位测试分析工作所得数据可以配套,并且有对比性,优先进行显微分光光度计的测试分析工作,然后再进行闪锌矿原位微量元素测试。

2.2 实验方法

2.2.1 偏光显微镜分析

光片、探针片的镜下观察在成都理工大学地球与行星科学学院综合岩矿鉴定实验室完成,偏光显微镜照相系统型号为NiKon LV100POL,搭载NiKon DS-Ri2影像系统。在综合岩矿鉴定实验室内,采用双层遮光窗帘(灰褐色窗帘和蓝色窗帘),保证镜下

观察的矿物不受影响。

2.2.2 闪锌矿显微分光光度分析

闪锌矿显微分光光度计测试分析在成都理工大学油气藏地质及开发工程全国重点实验室完成。使用的显微分光光度测试系统为德国Carl Zeiss有限公司和J&M公司联合生产的配备偏振光分析(A Pol)功能的Axio Scope. A1高分辨率显微镜与MSP 400光谱测量系统,由智能数码偏光显微镜和分光光度计组成,光源型号为HBO 100,光的接受元件为光电倍增管,内置多个曲面形状的倍增电极以及阳极和阴极(使发射的电子更好地聚焦),高倍镜下可测定小至0.5μm矿物颗粒。实验电源220V±10%、50Hz,测试温度25℃,相对湿度80%,放大倍数为10倍,测试束斑设置为与LA-ICP-MS原位微量测试的束斑直径较为接近的20μm×20μm。实验室使用双层遮光窗帘,外层浅蓝色,内层为红黑色,以扣除光谱干扰。

在测试之前,使用金刚石喷雾剂(粒度W=1μm)把所有抛光的样品表面重新抛光。将闪锌矿样品置于物台上,开启光度计,待仪器稳定后(30min)再开始标样校准及灵敏度调整,因测试对象为闪锌矿,测量波长范围调为可见光范围即可。为排除镜筒的界面对入射光产生耀光影响,调节分光光度计的测量光栏D₂,使D₂与视场光栏D₁的比值小于0.5。在实验中将检流计的读数调为100,依次读取400~700nm波长下闪锌矿的电流读数。每测试一组闪锌矿样品,再对标样矿物进行测试并读数。在测试工作中每隔15min重新对标样进行一次校准,标样参数列于表1。采用“平均白昼光影的选择波长坐标法”对反射率进行定量计算,具体方法见Hardy等^[22]。

2.2.3 闪锌矿原位微量元素分析

LA-ICP-MS原位微量元素含量测试在武汉上谱分析科技有限公司完成。GeolasPro激光剥蚀系统由COMPexPro 102 ArF 193nm准分子激光器和MicroLas光学系统组成,由Teledyne Cetac Technologies制造,型号为Analyte Excite。ICP-MS分析仪器采用Agilent 7700e电感耦合等离子体质谱仪(美国Agilent公司)。激光剥蚀过程中采用氦气作载气(370mL/min)、氩气为补偿气以调节灵敏度,二者在进入ICP之前通过一个T型接头混合,激光剥蚀系统配置有信号平滑装置,以保持剥蚀信号的稳定性。本次分析的激光束斑和频率分别为32μm和6Hz,能量密度3.0J/cm²,剥蚀样品信号40s,气体背景信号20s,洗脱气体信号30s。每10个测试点后加

表1 光度计标样在各波段反射率参数

Table 1 Reflectance parameters of photometer standard samples in different wavebands.

波长 (nm)	碳化硅介质反射率(%)		碳化钨介质反射率(%)	
	空气	油浸	空气	油浸
400	22.5	8.6	45.7	29.7
420	22.2	8.5	45.1	29.6
440	21.9	8.3	45.4	29.7
460	21.6	8.1	45.7	29.5
480	21.4	8.0	45.6	29.5
500	21.2	7.9	45.1	29.3
520	21.0	7.7	44.5	29.0
540	20.8	7.7	44.1	28.6
546	20.7	7.6	44.1	28.5
560	20.6	7.5	44.0	28.2
580	20.4	7.4	43.9	28.3
589	20.3	7.4	43.8	28.2
600	20.2	7.3	43.6	28.1
620	20.1	7.2	43.5	28.2
640	20.0	7.2	43.4	28.3
660	20.0	7.2	43.3	28.2
680	19.0	7.1	43.2	28.1
700	18.9	7.1	42.9	27.8

入1个NIST610(人工合成的硅酸盐玻璃标准物质)、2个MASS-1(硫化物标样)进行校正,采用“无内标基体归一法”对元素质量分数进行定量计算,具体方法见Liu等^[23]。

在ICP-MS分析中,氯化物、氧化物和双电荷离子会对主要元素的准确性产生干扰,因此通过剥蚀NIST610标准物质进行优化载气和补充气流,尽可能地减少基质引起的干扰。因为闪锌矿S、Fe元素含量在1%以上,而LA-ICP-MS测试检出限可达ng/g级,相差较大,因此采用自然丰度低的³⁴S、⁵⁷Fe进行检测。测定Ge元素时,Zn、Zr、Sm、Nd、Ce、Sn等元素的质谱峰叠加产生干扰,其中⁷⁰Zn、¹⁴⁰Ge²⁺会对⁷⁰Ge产生干扰,¹⁴⁴Sm²⁺、¹⁴⁴Nd²⁺会对⁷²Ge产生干扰,¹⁴⁸Sm²⁺、¹⁴⁸Nd²⁺会对⁷⁴Ge产生干扰。因为闪锌矿样品中Sm、Nd含量一般小于10μg/g,对比而言对⁷²Ge的干扰相对较小,且⁷²Ge也具有较高的灵敏度,所以选择⁷²Ge作为测量同位素。其余检测元素包括⁵⁵Mn、⁶³Cu、⁶⁶Zn、⁷¹Ga、¹⁰⁷Ag、¹¹¹Cd、²⁰⁴Pb、²⁰⁶Pb、²⁰⁷Pb、²⁰⁸Pb等。

2.3 测试数据处理

偏光显微镜拍摄照片利用NIS-Elements BR软件处理。

闪锌矿反射色颜色指数测试数据利用SpectraForensic软件处理。由于受闪锌矿中不可见

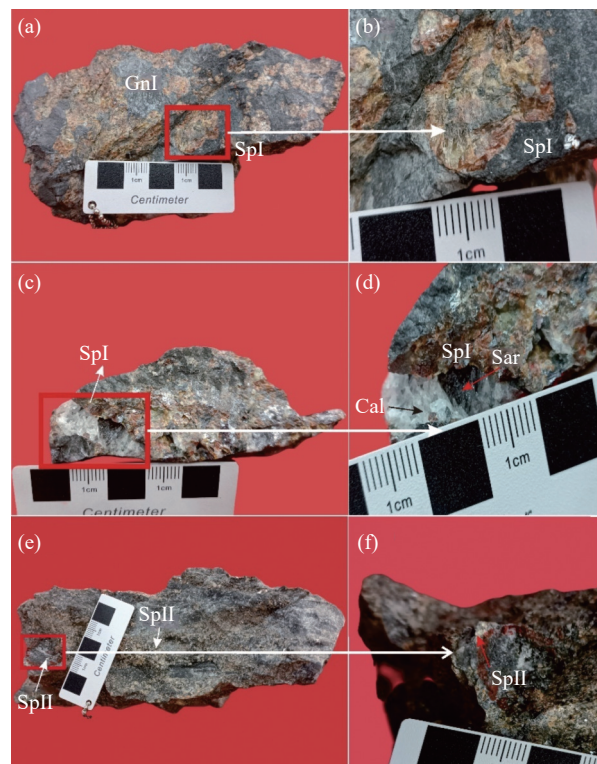
的微裂纹和内部反射色等因素的影响,反射率的测试值会略低于实际值,因此在测试结果中选取显微镜下干净光滑、靠近矿物颗粒中心的测试点。本次测试过程中标样矿物的相对误差小于1%,则测定的相对误差可以控制在2%以内;LA-ICP-MS微量元素测试数据的处理,包括对样品及空白信号的选择、仪器灵敏度的漂移校正、元素含量的计算,利用ICPMS DataCal软件完成。

3 样品分析结果

3.1 闪锌矿的特征及成矿期次

闪锌矿矿石构造以块状、浸染状、脉状为主(图2),矿石结构以它形粒状结构和半自形粒状结构为主(图3)。通过野外观察、手标本观察及镜下特征的鉴定,将热液期划分为两个阶段。

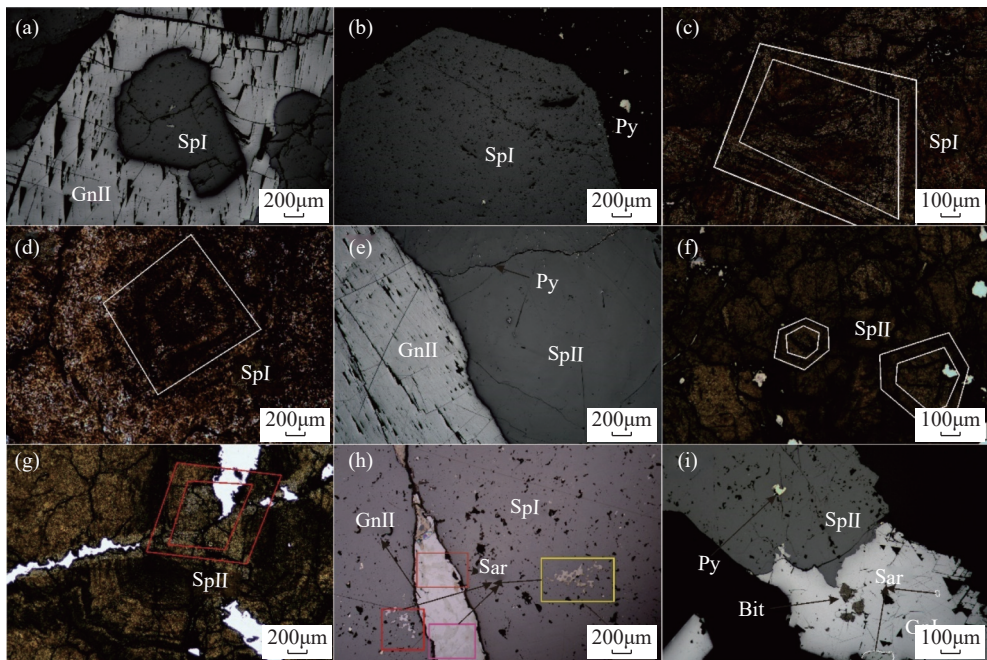
(1)白云石-石英-黄铁矿-闪锌矿I-方铅矿I阶段。I阶段闪锌矿(Sp I)矿石多呈块状、浸染状构造,闪锌矿多呈中-粗粒结构分布于矿石中,颜色较深,且颗粒较大(图2中a~d),在反射偏光显微镜下可见Sp I与黄铁矿紧密伴生,与I阶段方铅矿呈现共



Sp—闪锌矿; Gn—方铅矿; Cal—方解石; Sar—硫化物矿物。

图2 乌斯河矿床两阶段闪锌矿手标本特征

Fig. 2 Characteristics of sphalerite specimens in two stages of Wusihe deposit (Sp—Sphalerite; Gn—Galena; Cal—Calcite; Sar—Sulfide mineral).



(a) I阶段闪锌矿被Ⅱ阶段方铅矿交代,呈孤岛状; (b) Py的自形颗粒围绕I阶段自形闪锌矿的边缘分布; (c)、(d) I阶段闪锌矿的菱形环带; (e)Ⅱ阶段闪锌矿与Ⅱ阶段闪锌矿呈共边结构,有微细粒的Py颗粒沿闪锌矿裂隙分布; (f)、(g)Ⅱ阶段闪锌矿的多边形环带; (h)Ⅱ阶段方铅矿沿裂隙充填I阶段闪锌矿,硫化物矿物与Ⅱ阶段方铅矿伴生; (i)Ⅱ阶段闪锌矿交代I阶段方铅矿,硫化物矿物分布于方铅矿之上,呈浅绿色。Sp—闪锌矿; Gn—方铅矿; Py—黄铁矿; Bit—沥青; Sar—硫化物矿物。

图3 乌斯河矿床两阶段闪锌矿镜下特征

Fig. 3 Microscopic characteristics of sphalerite in two stages of Wusihe deposit.

边结构(图3中a,b),在透射偏光显微镜下可见闪锌矿具环带特征,震荡环带表现为自中心向外出现棕黑色、棕红色、橘红色的颜色交替的现象,韵律环带表现为自中心向边缘依次出现棕色、橘黄色、橘红色交替的现象(图3中c,d)。

(2)白云石-黄铁矿-闪锌矿Ⅱ-方铅矿Ⅱ-沥青-硫化物矿物阶段。Ⅱ阶段闪锌矿(SpⅡ)多呈中-细粒结构分布于矿石中(图2e),手标本上Ⅱ阶段闪锌矿颗粒颜色较浅,多见Ⅱ阶段矿脉切穿早期形成的围岩及矿层,在反射偏光显微镜下,可见Ⅱ阶段方铅矿与闪锌矿呈共边结构(图3e)。在透射偏光显微镜下也可见明显的环带结构,震荡环带表现为自中心向外出现棕黄色、黄色、黄白色的颜色交替的现象(图3中f,g)。

3.2 闪锌矿的反射色颜色指数

本次对矿床中两阶段闪锌矿的反射色颜色指数测试结果(表2)统计如下。SpⅠ的视觉反射率(R_{vis})范围为14.809%~16.890%,均值16.126%,SpⅡ的视觉反射率范围为15.657%~16.813%,均值16.187%;SpⅠ的反射色主波段(λ_d)范围为473.569~474.724nm,均值474.179nm,SpⅡ的反射色主波段范围为472.608~475.176nm,均值474.164nm;SpⅠ的颜色饱和度(P_e)范围为0.046~0.054,均值0.048,

表2 乌斯河矿床两阶段闪锌矿反射色颜色指数

Table 2 Reflected color index of sphalerite in two stages of Wusihe deposit.

样品编号	统计量	$R_{vis}(\%)$	$\lambda_d(\text{nm})$	P_e
SpⅠ-1 (n=4)	最小值	16.154	473.816	0.046
	最大值	16.386	474.724	0.048
	平均值	16.279	474.131	0.047
SpⅠ-2 (n=4)	最小值	14.809	473.569	0.048
	最大值	16.890	474.543	0.054
	平均值	15.974	474.226	0.050
SpⅡ-1 (n=3)	最小值	15.657	473.988	0.040
	最大值	16.190	475.176	0.043
	平均值	15.961	474.445	0.042
SpⅡ-2 (n=4)	最小值	15.990	472.608	0.044
	最大值	16.813	475.145	0.045
	平均值	16.367	473.954	0.044

SpⅡ的颜色饱和度范围为0.040~0.045,均值0.043。对比两阶段闪锌矿的颜色指数特征(图4),两阶段的视觉反射率、反射色主波段相差不大,但在反射色饱和度上SpⅠ明显高于SpⅡ。

3.3 闪锌矿的原位微量元素特征

本次选取乌斯河铅锌矿床的两阶段闪锌矿开展LA-ICP-MS原位微量元素含量测试,结果列于表3。

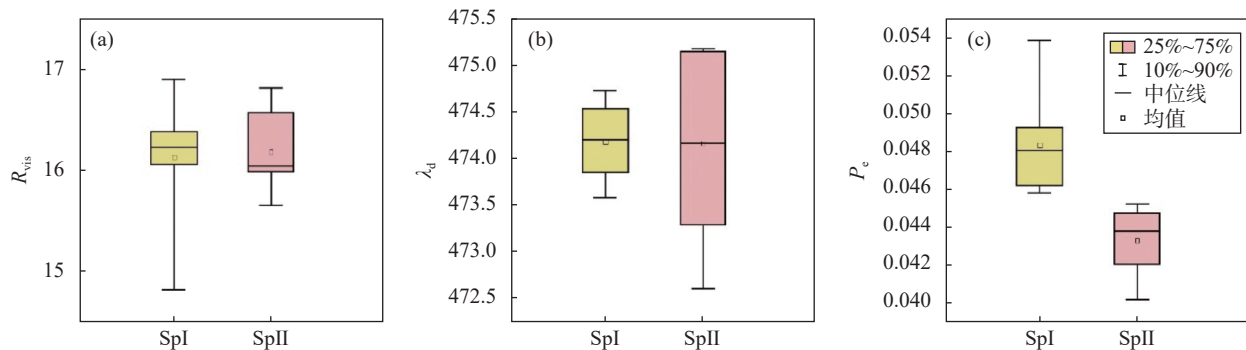


图4 乌斯河矿床两阶段闪锌矿视觉反射率(a)、反射色主波段(b)、反射色饱和度(c)箱型图

Fig. 4 Box diagrams of visual reflectance (a), reflected color main band (b) and reflected color saturation (c) of sphalerite in two stages of Wusihe deposit.

表3 乌斯河矿床两阶段闪锌矿微量元素特征数据($\times 10^{-6}$)

Table 3 Data of trace element characteristics of sphalerite in two stages of Wusihe deposit ($\times 10^{-6}$).

元素	含量单位	Sp I 阶段(n=12)				Sp II 阶段(n=11)			
		最大值	最小值	平均值	标准偏差	最大值	最小值	平均值	标准偏差
Mn	10^{-6}	59.46	11.32	37.55	16.07	17.94	3.22	10.81	5.29
Fe	10^{-2}	2.72	0.44	1.52	0.66	0.76	0.11	0.32	0.22
Cu	10^{-6}	857.74	33.55	234.30	244.40	240.21	4.96	78.02	57.32
Ga	10^{-6}	19.12	0.05	5.84	7.79	40.12	0.44	19.09	13.44
Ge	10^{-6}	624.21	96.25	244.33	178.97	169.17	1.54	43.22	42.80
Ag	10^{-6}	94.93	30.14	53.65	24.20	95.74	5.49	41.92	23.35
Cd	10^{-6}	3589.09	33.75	1506.86	1230.18	9061.67	1276.70	3681.55	2549.88
In	10^{-6}	0.23	—	0.08	0.09	0.26	—	0.10	0.10
Pb	10^{-6}	1863.47	24.10	412.53	508.17	459.49	82.75	261.52	127.07

注: “—”表示低于检出限, 未检出。

两阶段闪锌矿中 Ge 平均含量变化范围较大, 不同阶段的闪锌矿中 Ge 含量有所不同, Sp I 中 Ge 含量变化范围为 $96.25 \times 10^{-6} \sim 624.21 \times 10^{-6}$, 均值 244.33×10^{-6} ; Sp II 中 Ge 含量变化范围为 $1.54 \times 10^{-6} \sim 169.17 \times 10^{-6}$, 均值 43.22×10^{-6} ; Sp I 中 Ge 含量高于 Sp II。除 Ge 外, 其他元素在不同阶段闪锌矿中的含量特征也有所不同。

Sp I 阶段中, Fe 含量介于 $0.44\% \sim 2.72\%$, 均值 1.52% ; Cd 含量介于 $33.75 \times 10^{-6} \sim 3589.09 \times 10^{-6}$, 均值为 1506.86×10^{-6} ; Mn 含量介于 $11.32 \times 10^{-6} \sim 59.46 \times 10^{-6}$, 均值 37.55×10^{-6} ; Cu 含量介于 $33.55 \times 10^{-6} \sim 857.74 \times 10^{-6}$, 均值 234.30×10^{-6} ; Ga 含量介于 $0.05 \times 10^{-6} \sim 19.12 \times 10^{-6}$, 均值 5.84×10^{-6} ; Ag 含量介于 $30.14 \times 10^{-6} \sim 94.93 \times 10^{-6}$, 均值 53.65×10^{-6} ; In 含量部分测点低于检测线, 最高值 0.23×10^{-6} , 均值 0.08×10^{-6} ; Pb 含量介于 $24.10 \times 10^{-6} \sim 1863.47 \times 10^{-6}$, 均值 412.53×10^{-6} 。

Sp II 阶段中, Fe 含量介于 $0.11\% \sim 0.76\%$, 均值 0.32% ; Cd 含量介于 $1276.70 \times 10^{-6} \sim 9061.67 \times 10^{-6}$, 均值 3681.55×10^{-6} ; Mn 含量介于 $3.22 \times 10^{-6} \sim 17.94 \times 10^{-6}$, 均值 10.81×10^{-6} ; Cu 含量介于 $4.96 \times 10^{-6} \sim 240.21 \times 10^{-6}$, 均值 78.02×10^{-6} ; Ga 含量介于 $0.44 \times 10^{-6} \sim 40.12 \times 10^{-6}$, 均值 19.09×10^{-6} ; Ag 含量介于 $5.49 \times 10^{-6} \sim 95.74 \times 10^{-6}$, 均值 41.92×10^{-6} ; In 含量部分测点低于检出限, 最高值 0.26×10^{-6} , 均值 0.10×10^{-6} ; Pb 含量介于 $82.75 \times 10^{-6} \sim 459.49 \times 10^{-6}$, 均值 261.52×10^{-6} 。

4 富锗闪锌矿标型特征的指示意义

4.1 闪锌矿矿物标型与锗的关系

4.1.1 锗的赋存状态与替代方式

在铅锌矿床中, Ge 主要以类质同象的方式进入闪锌矿晶格, 少数以独立矿物的形式存在^[3, 18]。乌斯河矿床中两阶段闪锌矿的时间分辨率曲线上(图 5), 元素 Fe、Ge、Cu、Pb、Ag 的曲线趋势与 Zn

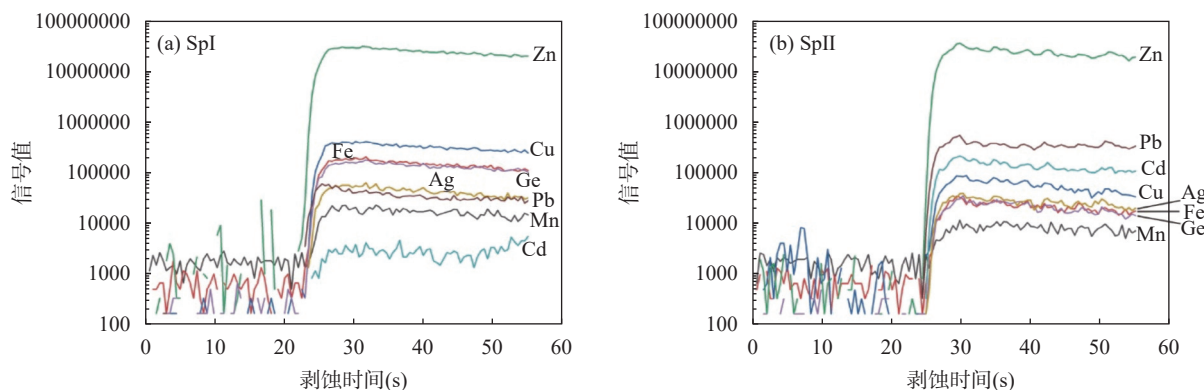


图5 乌斯河矿床 Sp I 阶段(a)和 Sp II 阶段(b)闪锌矿的微量元素时间分辨率曲线

Fig. 5 Time resolution curves of trace elements of Sp I stage (a) and Sp II stage (b) sphalerite in Wusihe deposit.

一致,说明包括Ge元素在内的这5种元素在闪锌矿晶体中占据了一定的空间位置。

从Ge元素本身的性质来看,Ge为亲硫元素,且Ge离子半径大小与Zn离子半径相近(Zn^{2+} =75pm, Ge^{2+} =73pm, Ge^{4+} =54pm),因此Ge以类质同象的形式替代Zn进入闪锌矿中是可行的。目前,关于Ge的替代方式主要有8种:① $Ge^{4+}+2Fe^{2+}+\gamma$ (γ 空位) $\leftrightarrow 4Zn^{2+}$ ^[24];② $Ge^{4+}+\gamma \leftrightarrow 2Zn^{2+}$ 或 $Ge^{2+} \leftrightarrow Zn^{2+}$ ^[5];③ $nCu^{2+}+Ge^{2+} \leftrightarrow (n+1)Zn^{2+}$ ^[3];④ $2Cu^{+}+Cu^{2+}+Ge^{4+} \leftrightarrow 4Zn^{2+}$ ^[7];⑤ $Ge^{4+}+2(Cu^{+}, Ag^{+}) \leftrightarrow 3Zn^{2+}$ ^[24];⑥ $Ge^{2+}+Mn^{2+} \leftrightarrow 2(Zn, Cd)^{2+}$ ^[9];⑦ $Fe^{2+}+Ge^{2+} \leftrightarrow 2Zn^{2+}$ ^[9];⑧ $2Cu^{+}+Ge^{4+} \leftrightarrow 3Zn^{2+}$ ^[9,18]。

Liu等^[25]通过微束X射线近边吸收结构分析(μ -XANES)发现Ge在闪锌矿中主要以 Ge^{4+} 的形式存在。通过Ge与Fe、Cu、Ag等元素的相关性分析(图6),Ge与Fe之间没有明显相关性,与Cu之间有一定程度的正相关性($R^2>0.6$),Ge与Ag的相关性在两阶段闪锌矿中出现了明显的不同,I阶段闪锌矿中Ge与Ag没有显著的相关性,II阶段闪锌矿中Ge与Ag则具有一定程度的正相关性($R^2>0.6$)。结合微量元素数据,I阶段闪锌矿中Ge、Cu含量高于II阶段闪锌矿,两阶段闪锌矿中Ag含量没有明显区别。推测在Cu含量高时,Ge优先与Cu一起参与反应;当Cu离子浓度下降后,Ge才开始与Ag离子一起参与反应。因此,在第I阶段当Cu离子浓度较高时,优先存在替代方式⑧ $2Cu^{+}+Ge^{4+} \leftrightarrow 3Zn^{2+}$,当流体中Cu离子浓度降低时,出现第II阶段的替代方式⑤ $Ge^{4+}+2(Cu, Ag)^{+} \leftrightarrow 3Zn^{2+}$ 。

4.1.2 闪锌矿中锗的分布

乌斯河矿床中的闪锌矿多发育环带结构,深色的Sp I被浅色的Sp II包围,形成了由内向外颜色依

次变浅的多阶段闪锌矿环带(图7)。由图可见,随着环带颜色由深至浅的变化,Fe、Cu、Mn、Ge含量均呈现先下降再上升的变化趋势,其中与Ge含量变化趋势最为相近的元素是Cu、Ag,图中4号点以后随着Cu含量下降,Ag含量的变化趋势逐渐与Cu重合,与Ge含量的变化趋势相似,符合在4.1.1节中讨论Ge在第I、II阶段闪锌矿中的替代方式的结果。而Fe与Mn变化趋势相似,二者都与Ge的变化趋势相差较大。

两阶段闪锌矿中Ge的含量差异在环带中的表现方式是,Ge更倾向于在颜色较深、反射色饱和度较高闪锌矿中(Sp I)富集。

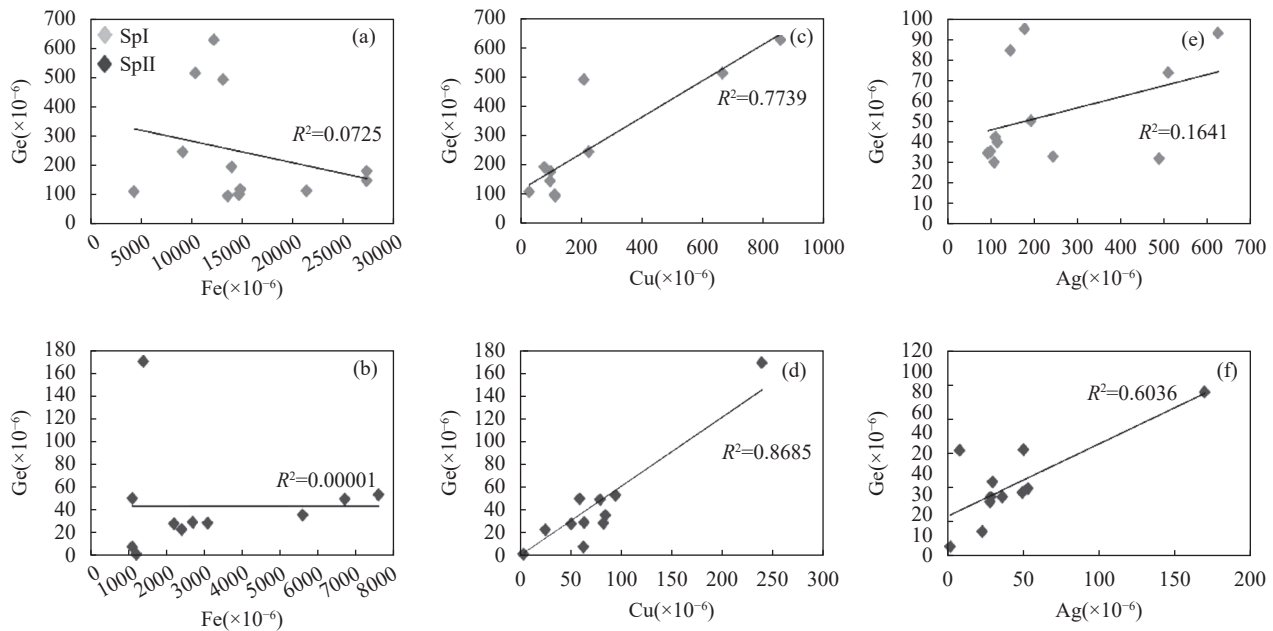
4.2 闪锌矿矿物标型与成矿温度

4.2.1 闪锌矿的晶体形态特征与成矿温度的关系

闪锌矿属等轴晶系,为离子晶体结构,其晶体形态与温度有着密切的联系,通常呈立方体、四面体习性产出的,一般为高温下形成的闪锌矿,而以菱形十二面体习性产出的则为中-低温下形成的闪锌矿^[26]。在采集样品中,可见较为完整的菱形十二面体晶型的闪锌矿颗粒(图2中e,f),且自形程度较高的闪锌矿常见其出现六边形切面及菱形切面(图3中c,d),指示矿床的成矿温度应为中-低温。

4.2.2 闪锌矿的反射色颜色指数与成矿温度的关系

闪锌矿的反射色是具化的矿物本身化学成分及物理性质的外部现象,而矿物的反射色又可以被颜色指数表征,因此矿物的反射色颜色指数可以在一定程度上反映矿物的物理性质与化学成分之间的联系。Lai等^[6]通过总结Fe-Cu-Zn-S和Fe-Zn-S体系中闪锌矿成矿温度、FeS分子摩尔百分含量(FeS mol%)、硫逸度以及反射色颜色指数之间的关系,得出通过闪锌矿的反射色颜色指数计算闪锌矿成矿时



(a)、(b) 为两阶段闪锌矿中 Fe-Ge 元素关系; (c)、(d) 为两阶段闪锌矿中 Cu-Ge 元素关系; (e)、(f) 为两阶段闪锌矿中 Ag-Ge 元素关系。

图6 乌斯河矿床两阶段闪锌矿微量元素关系

Fig. 6 Relationship of trace elements of sphalerite in two stages of Wusihe deposit.

温度上限的计算公式为:

$$T (\text{°C}) = 61.4 \times R_{\text{vis}} + 1.1 \times \lambda_d + 6000 \times P_e - 1533 \quad (1)$$

式中: R_{vis} 表示视觉反射率; λ_d 表示反射色主波段; P_e 表示颜色饱和度。

利用上述公式(1)计算得到乌斯河铅锌矿床中两阶段闪锌矿的最高成矿温度,其中 Sp I 的成矿温度上限范围为 203.0~293.0°C,平均温度 268.7°C; Sp II 的成矿温度上限范围为 221.2~280.4°C,平均温度 242.0°C。因此,乌斯河矿床的成矿上限温度也属中-低温,且 Sp I 的成矿最高温度略高于 Sp II。

4.2.3 闪锌矿微量元素组成特征与成矿温度的关系

闪锌矿中的微量元素组成对成矿温度具有一定的指示意义^[27-28]。在高温条件下,闪锌矿一般容易富集 Fe,并将 Fe 含量大于 15% 的闪锌矿称为铁闪锌矿^[29]。乌斯河铅锌矿床中两阶段闪锌矿的 Fe 含量分别为: 0.44%~2.72%(均值 1.52%)、0.11%~0.76%(均值 0.32%);两阶段闪锌矿的 Fe 含量均低于 15%,指示成矿温度属中-低温范畴。此外,微量元素 Ga/In 的比值也可指示闪锌矿成矿时的温度。若 $0.01 < \text{Ga/In} < 0.05$, 则指示闪锌矿的成矿温度为高温;若 $0.01 < \text{Ga/In} < 5$, 则指示其成矿温度为中温;若 $1 < \text{Ga/In} < 100$ 则指示其成矿温度为低温^[26]。乌斯河矿床两阶段闪锌矿的 Ga/In 比值范围分别为

1.09~143、41~211。Frenzel 等^[30]对全球各类成因的铅锌矿床中闪锌矿的微量元素组成进行了统计学分析,基于闪锌矿中 Fe、Mn、Ga、In、Ge 的质量分数建立了一个用于计算矿床形成温度的经验公式,该公式是通过统计多个矿床的流体包裹体的均一温度建立的,所以该公式所得的温度估算结果接近于成矿温度的下限,计算公式如下:

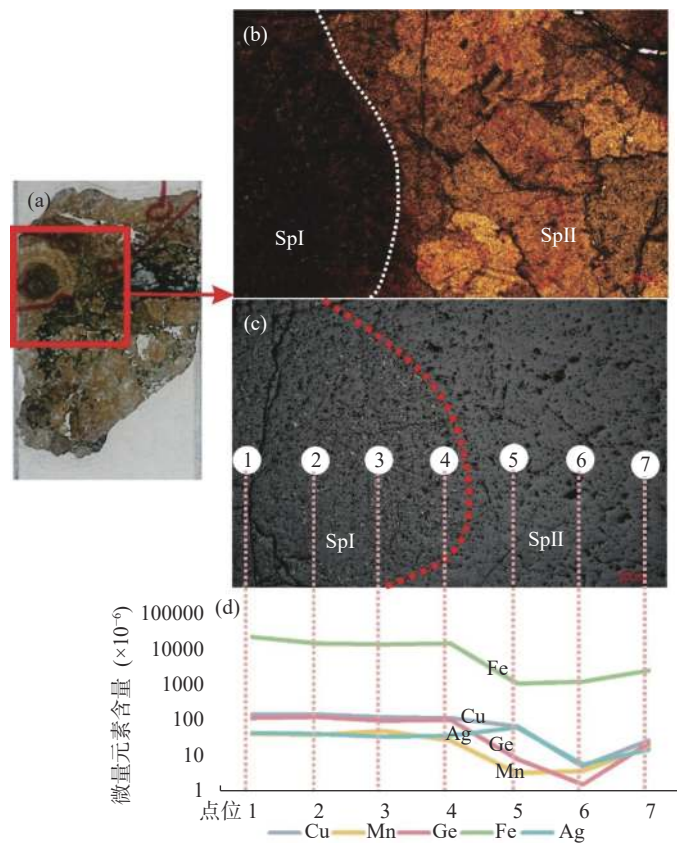
$$\text{PC1}^* = \frac{C_{\text{Ga}}^{0.22} \times C_{\text{Ge}}^{0.22}}{C_{\text{Fe}}^{0.37} \times C_{\text{Mn}}^{0.20} \times C_{\text{In}}^{0.11}} \quad (2)$$

$$T (\text{°C}) = -(54.4 \pm 7.3) \times \text{PC1}^* + (208 \pm 10) \quad (3)$$

式中: PC1^* 表示其主成分分析结果中的第一个主成分; C_a^b 表示元素 a 的浓度, Ga、Ge、Mn、In 浓度单位为 $\mu\text{g/g}$, Fe 浓度单位为质量分数 %; 系数 b 等于元素 a 的含量与其对数标准差的比值。

利用上述公式(2)和(3)计算得到乌斯河矿床两阶段闪锌矿的成矿温度分别为: Sp I 温度范围 87.7~189°C(平均 146°C); Sp II 温度范围 83.3~199°C(平均 137°C)。

综合上述晶体形态、反射色颜色指数特征、微量元素比值所指示的乌斯河矿床闪锌矿的成矿温度,矿床应属中-低温矿床,与熊索菲等^[15]在对该矿床中的白云石、闪锌矿、石英的流体包裹体显微测温得到成矿流体为中-低温流体的结果一致。就两阶段闪



(a) 闪锌矿环带探针片照片; (b) 闪锌矿环带透射偏光镜下照片; (c) 闪锌矿环带反射偏光镜下照片; (d) 闪锌矿环带 LA-ICP-MS 测试点位(1~7)与元素含量折线图。

图7 乌斯河矿床闪锌矿环带及微量元素折线图

Fig. 7 Line diagrams of sphalerite gird and trace elements in Wusihe deposit.

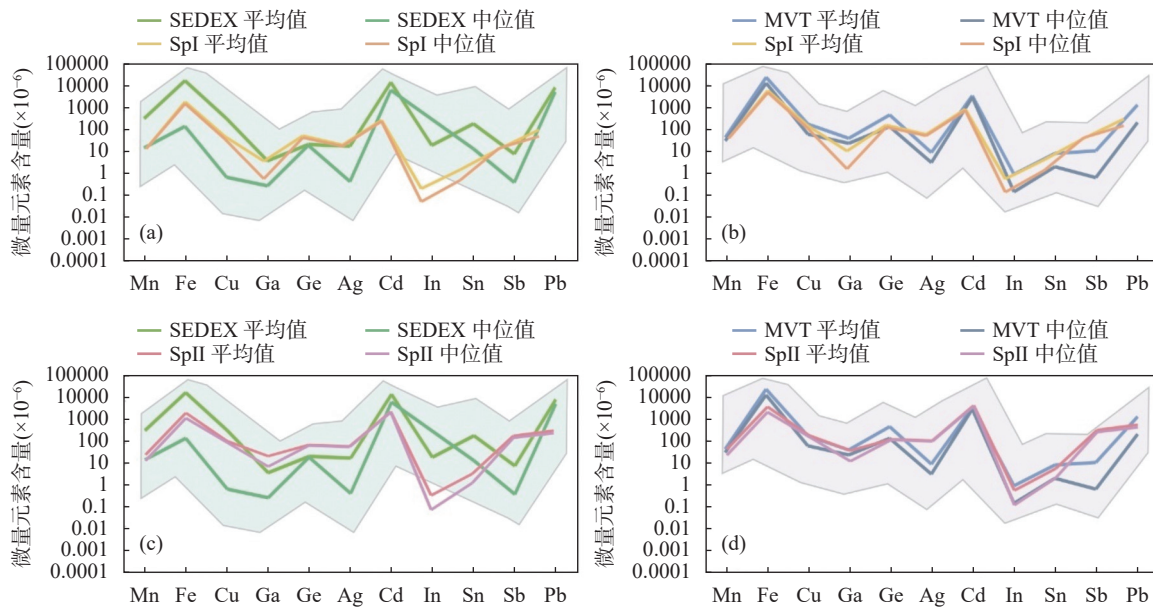
锌矿来看, Sp I 至 Sp II 应属一个降温的过程, 但乌斯河矿床中 Sp I 中 Ge 的含量高于 Sp II, 这与“低温条件下, Ge 更易富集”相矛盾^[30]。罗开等^[18]统计了包括乌斯河在内的富 Ge 铅锌矿床 Ge 含量与温度的关系, 发现成矿温度与 Ge 含量变化并不存在明显的关系。但在目前已知的富 Ge 铅锌矿床都属于中-低温矿床, 因此温度必然与 Ge 的富集存在某种联系。在 4.1.1 节讨论中 Ge 在两阶段闪锌矿的替代方式发生了改变, Sp II 阶段闪锌矿中与 Ge 元素协同替代闪锌矿晶格中 Zn 元素的 Cu 元素明显降低, 导致在温度更低的 Sp II 闪锌矿中富集 Ge 相对较低一些。此外, 在成矿过程中随着金属离子不断析出, 流体中的 Ge 的离子活度也会降低。

4.3 闪锌矿矿物标型特征与矿床成因的判别

目前针对乌斯河铅锌矿床的成因主要集中在两种类型: SEDEX 矿床^[12] 和 MVT 矿床^[14, 16-18]。研究表明, 不同矿床中某些特定元素的含量不同(如 Mn、Fe、Cu、Ge 等)^[31]。就乌斯河矿床的成因类型,

以闪锌矿的微量元素特征对矿床的成因进行判别, 结果如图 8 所示。在图 8 中, 乌斯河矿床两阶段闪锌矿的微量元素平均值折线及中位数折线均与 MVT 型矿床的折线走势相同, 而与 SEDEX 型矿床的折线走势不同, 且两阶段闪锌矿的中位数及平均值折线图的取值范围也与 MVT 型矿床的范围重叠率更高, 与 SEDEX 型矿床的重叠率较 MVT 型矿床低。因此, 就两阶段闪锌矿的微量元素特征来看, 乌斯河矿床的成因类型更接近于 MVT 型。

Lai 等^[6]发现闪锌矿的反射色颜色指数与闪锌矿的这些特定元素大多密切相关, 再通过因子分析创建了判断矿床成因的指示图, 可作为判断铅锌矿床成因的重要依据。因此, 将乌斯河矿床两阶段闪锌矿的反射色颜色指数特征进行投图, 这种方式来为判别矿床成因类型提供理论依据, 结果如图 9 所示。投点绝大部分落在了 MVT 型矿床的区域, 仅一个点落在各种成因类型矿床的重叠区域, 该点可能是由于测量时的误差所致, 且落点区域与 SEDEX 型



(a) Sp I 与 SEDEX 型矿床的微量元素特征对比; (b) Sp II 与 SEDEX 型矿床的微量元素特征对比; (c) Sp I 与 MVT 型矿床的微量元素特征对比; (d) Sp II 与 MVT 型矿床的微量元素特征对比。MVT 型、SEDEX 型矿床闪锌矿原位微量数据来自文献 [5-6, 31-34] 。

图8 闪锌矿微量元素特征成因类型判别图解

Fig. 8 Identification diagrams of genetic types of trace elements in sphalerite.

矿床的区域相差甚远。因此,乌斯河铅锌矿床应不属于 SEDEX 铅锌矿床。

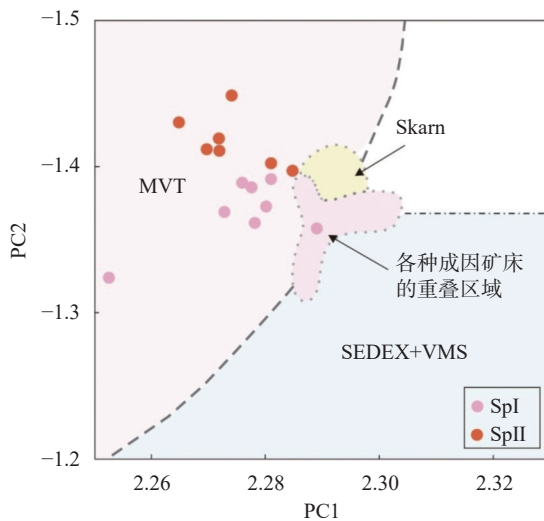


图9 闪锌矿颜色指数特征成因类型判别图解

(底图据 Lai 等 [6] , $\log(\lambda_d)$ 、 $\log(R_{vis})$ 、 $\log(P_e)$ 在 PC1 上的得分系数分别为 0.584、0.584、-0.005, 在 PC2 上的得分系数分别为 0.055、-0.047、0.996)

Fig. 9 Genetic type discrimination diagram of color index characteristics of sphalerite (Modified by Lai, et al [6] . The score coefficients of $\log(\lambda_d)$, $\log(R_{vis})$ and $\log(P_e)$ on PC1 are 0.584, 0.584 and -0.005, respectively, and those on PC2 are 0.055, -0.047 and 0.996, respectively).

5 结论

以扬子地块西南缘乌斯河铅锌矿床富 Ge 闪锌矿为研究对象,采用显微分光光度计、LA-ICP-MS 两种测试方法,以及偏光显微镜下观察进行矿物标型研究。研究结果表明,乌斯河铅锌矿床热液成矿期发育两个阶段的富 Ge 闪锌矿,其 Ge 的富集程度及替代方式存在差异,替代方式分别为 $Ge^{4+} + 2Cu^{+} \leftrightarrow 3Zn^{2+}$, $Ge^{4+} + 2(Cu, Ag)^{+} \leftrightarrow 3Zn^{2+}$, 认为 Ge 更易在反射色饱和度高的闪锌矿 (Sp I) 中富集。富 Ge 闪锌矿的微量元素特征、颜色指数及晶体形态均反映了该矿床成矿温度为中-低温,矿床类型为 MVT 型铅锌矿床。

显微分光光度计可以有效地测定闪锌矿的反射色颜色指数特征,显微分光光度计和 LA-ICP-MS 两种方法将闪锌矿的光学性质与化学成分结合起来进行分析,对进一步认识富锗铅锌矿床具有重要的研究意义,对其他金属矿物也有较好的应用前景。

致谢:感谢成都理工大学地球与行星科学学院张燕高级实验师提供的帮助。

Mineral Typomorphic Characteristics and Deposit Genesis of Germanium-Enriched Sphalerite from Wusihe in the Southwestern Margin of the Yangtze Block

SUN Shiqiang, CHEN Cuihua*, ZHAO Wenhao, LAI Xiang, MA Tianqi, ZHANG Haijun, QIAO Mengyi, SONG Zhijiao, CHEN Xiaojie, GU Ying

(School of Earth and Planetary Sciences, Chengdu University of Technology, Chengdu 610059, China)

HIGHLIGHTS

- (1) Microscopic spectrophotometry and LA-ICP-MS analysis were used to quantitatively analyze the physical color and chemical trace elements of Ge-enriched sphalerite, and the differential enrichment of Ge was found in two-stage sphalerite.
- (2) Ge exists in the form of isomorphism in two-stage sphalerite, with replacement of $2\text{Cu}^{+} + \text{Ge}^{4+} \leftrightarrow 3\text{Zn}^{2+}$ and $\text{Ge}^{4+} + 2(\text{Cu}, \text{Ag})^{+} \leftrightarrow 3\text{Zn}^{2+}$, respectively.
- (3) Ge is more easily enriched in sphalerite with high reflective color saturation, and the mineral type of sphalerite indicates that the deposit should be of medium low temperature and Mississippi Valley-type.

ABSTRACT: The Wusihe lead-zinc deposit, situated at the southwestern margin of the Yangtze Block and a prominent Ge-enriched deposit within the Sichuan—Yunnan—Guizhou lead-zinc metallogenic belt, faces ongoing debates regarding its genesis. The influence of sphalerite typomorphic characteristics on Ge enrichment and substitution mechanisms within the deposit remains a crucial puzzle to unravel. To address this, the paper employs quantitative analyses using microscopic spectrophotometry and laser ablation-inductively coupled plasma-mass spectrometry (LA-ICP-MS). The results reveal the presence of two sphalerite stages during the hydrothermal period: a darker Stage I and a lighter Stage II. Despite similar mean values for visual reflectance and the dominant wavelength of reflectance color, the mean reflectance color saturation differs (0.048 and 0.043, respectively), with corresponding average Ge contents of $244.33 \times 10^{-6} \mu\text{g/g}$ and $43.22 \times 10^{-6} \mu\text{g/g}$, respectively. The experimental outcomes conclude that Ge exists in sphalerite as isomorphism and is more concentrated in sphalerite with higher reflectance color saturation. The ore-forming temperature is medium to low, classifying the deposit as a Mississippi Valley-type lead-zinc deposit. The BRIEF REPORT is available for this paper at <http://www.ykcs.ac.cn/en/article/doi/10.15898/j.ykcs.202406210138>.

KEY WORDS: Ge-enriched lead zinc deposit; characteristics of sphalerite morphology; substitution mechanisms; microscopic spectrophotometer; laser ablation-inductively coupled plasma-mass spectrometry; isomorphism; Mississippi Valley-type lead-zinc deposit

BRIEF REPORT

Significance: Germanium (Ge) is widely used in important fields such as semiconductors, infrared optics, optical fibers, polymerization catalysts, and medicine, due to its excellent thermal conductivity, electrical conductivity, high refractive index, and low dispersion properties^[1-2]. Notably, nearly three-quarters of industrial Ge worldwide is sourced from sphalerite in lead-zinc deposits^[3-4]. The mineralogical typomorphic characteristics of sphalerite can often effectively reflect the formation environment and genetic type of the deposit^[5-6]. Therefore, conducting deep research on the enrichment mechanism of Ge in lead-zinc deposits and the typomorphic features of Ge-enriched sphalerite is not only significant for further understanding the mineralization patterns of Ge-enriched lead-zinc

deposits, but also holds practical value for the exploration and development of Ge resources.

The Wusihe lead-zinc deposit, located on the southwestern edge of the Yangtze Block, is an important lead-zinc polymetallic deposit in the Sichuan—Yunnan—Guizhou metallogenic belt. Experts and scholars have gained a deep understanding of its metallogenic geological background^[13], sources of metallogenic materials^[14-15], characteristics of metallogenic fluids^[14,16], petrogeochemical features^[14-16], and deposit genesis^[13-18]. Luo et al.^[18] also discovered differential enrichment of Ge in sphalerite from different stages within this deposit. Whether the typomorphic characteristics of sphalerite affect the enrichment of Ge remains worthy of further investigation. Additionally, there are still two differing views on the genesis of the Wusihe lead-zinc deposit: one as a sedimentary exhalative (SEDEX) deposit^[13] and the other as a Mississippi Valley-type (MVT) deposit^[14,16-18].

Therefore, focusing on typomorphic characteristics of Ge-enriched sphalerite and the genesis of the deposit in this area, two testing methods are primarily adopted: microscopic spectrophotometry and LA-ICP-MS. Based on the test results, it investigate the relationship between the mineral typomorphic characteristics of sphalerite and the enrichment of Ge, as well as the implications of the former for ore-forming temperatures and the genesis of ore deposits. Research finds that microscopic spectrophotometry can quantitatively measure the visual reflectance (R_{vis}), dominant reflectance wavelength (λ_d), and mean reflectance saturation (P_e) of sphalerite. These characteristics of sphalerite have certain indicative significance for ore-forming temperatures, types of ore deposit genesis, and element enrichment patterns. Sphalerite with high P_e value is more enriched in Ge, and the ore deposit has a medium-to-low ore-forming temperature with a MVT genesis.

Methods: The experimental samples were primarily sourced from the Wusihe lead-zinc deposit located on the north bank of the Dadu River. Based on field geological investigations, systematic sampling was conducted in mining areas 1, 2, 5, and 12 (as shown in Fig.1c). The preparation of thin sections and probe slices was completed at the Rock and Mineral Testing Center of the Hebei Geological Survey and Mapping Institute, with the thin sections polished to dimensions of 3.7cm×2.6cm×0.6cm and the probe slices to a thickness of 150μm.

Microscopic observations of the thin sections and probe slices were performed at the Comprehensive Rock and Mineral Identification Laboratory of the College of Earth and Planetary Sciences, Chengdu University of Technology, using a NiKon LV100POL polarized light microscope equipped with a NiKon DS-Ri2 imaging system.

In situ spectrophotometric analysis of sphalerite was conducted at the National Key Laboratory of Oil and Gas Reservoir Geology and Development Engineering, Chengdu University of Technology. The spectrophotometric testing system used was the Axio Scope.A1 high-resolution microscope equipped with polarized light analysis functionality, jointly produced by Carl Zeiss GmbH and J&M, and paired with the &MSP 400 spectral measurement system. The light source model was HBO 100, and the light-receiving element was a photomultiplier tube containing multiple curved-surface shaped dynodes, an anode, and a cathode, capable of measuring mineral particles as small as 0.5μm under high magnification. The test beam spot was set to 20μm×20μm. The laboratory used double-layered light-blocking curtains, with an outer layer of light blue and an inner layer of red-black, to subtract spectral interference. Before testing, all polished sample surfaces were re-polished using diamond spray (grain size $W=1\mu\text{m}$). The spectrophotometer was turned on, and after the instrument stabilized (30min), standard sample calibration and sensitivity adjustments were performed. During testing, the standard sample was recalibrated every 15min, and the standard sample parameters are listed in Table 1. Quantitative calculation of reflectance was performed using the “Selective Wavelength Coordinate Method for Average Daylight” as described by Hardy et al^[24].

LA-ICP-MS *in situ* trace element content testing was completed at the Wuhan Shangpu Analysis Technology Co., Ltd. The GeolasPro laser ablation system consisted of a COMPexPro 102 ArF 193nm excimer laser and MicroLas optical system, manufactured by Teledyne Cetac Technologies, model Analyte Excite. The ICP-MS analyzer used was the Agilent 7700e Inductively Coupled Plasma-Mass Spectrometer (Agilent Corporation, USA).

During laser ablation, helium was used as the carrier gas (370mL/min), and argon as the compensation gas to adjust sensitivity. Both gases were mixed through a T-connector before entering the ICP. The laser ablation system was equipped with a signal smoothing device to maintain the stability of the ablation signal. The laser beam spot and frequency used in this analysis were 32 μm and 6Hz, respectively, with an energy density of 3.0J/cm². The ablation sample signal duration was 40s, the gas background signal duration was 20s, and the washout gas signal duration was 30s. After every 10 test points, 1 NIST610 (synthetic silicate glass standard material), and 2 MASS-1 (sulfide standard samples) were added for correction. Quantitative calculation of element mass fractions was performed using the “Internal Standard-Free Matrix Normalization Method” as described by Liu et al^[23].

Photographs taken with the polarized light microscope were processed using NIS-Elements BR software; LA-ICP-MS trace element test data were processed using ICPMS DataCal software; sphalerite reflectance color index test data were processed using Spectra Forensic software. During this testing process, if the relative error of the standard sample minerals was less than 1%, the measured relative error could be controlled within 2%.

Data and Results: The test results obtained using a microspectrophotometer (Table 2) reveal that the average R_{vis} values for the two stages of sphalerite (Sp I and Sp II) are 16.126% and 16.187%, respectively; the average λ_d values are 474.179nm and 474.164nm, respectively; and the average P_e values are 0.048 and 0.043, respectively. The LA-ICP-MS test results (Table 3) indicate that the Ge contents of Sp I and Sp II are 244.33×10^{-6} and 43.22×10^{-6} , respectively. In the test results of the microspectrophotometer, the error of visual reflectance is less than 0.3%, the error of the main band of reflection color is less than 1nm, and the error of color saturation is less than 0.001. In the test results of the microspectrophotometer, there is little difference in visual reflectance and the main band of reflection color among different stages of sphalerite, but there is a relatively large difference in color saturation. Compared with Lai et al^[6] test results for four lead-zinc deposits, it also shows the characteristics of little difference in visual reflectance and the main band of reflection color, but a relatively large difference in color saturation, which may be due to the characteristics of sphalerite itself. The detection limit of LA-ICP-MS can reach the ng/g level, with significant differences. Therefore, ³⁴S and ⁵⁷Fe with low natural abundance are used for detection. When measuring the element Ge, the mass spectral peaks of elements such as Zn, Zr, Sm, Nd, Ce, and Sn overlap and cause interference. Specifically, ⁷⁰Zn and ¹⁴⁰Ge²⁺ interfere with ⁷⁰Ge, ¹⁴⁴Sm²⁺ and ¹⁴⁴Nd²⁺ interfere with ⁷²Ge, and ¹⁴⁸Sm²⁺ and ¹⁴⁸Nd²⁺ interfere with ⁷⁴Ge. Because the content of Sm and Nd in sphalerite samples is generally less than 10 $\mu\text{g}/\text{g}$, the interference on ⁷²Ge is relatively small. Moreover, ⁷²Ge also has high sensitivity, so ⁷²Ge is selected as the measurement isotope. Other detected elements include ⁵⁵Mn, ⁶³Cu, ⁶⁶Zn, ⁷¹Ga, ¹⁰⁷Ag, ¹¹¹Cd, ²⁰⁴Pb, ²⁰⁶Pb, ²⁰⁷Pb, ²⁰⁸Pb, etc. The spot size selected for LA-ICP-MS testing is 32 μm , which is closer to the spot size (20 μm) of the microspectrophotometer, ensuring the accuracy of trace element test results and a higher degree of matching with the test results of the microspectrophotometer.

参考文献

- [1] 刘萧晗, 孟郁苗. “锗”里有奥秘, 观“锗”寻真谛[J]. *矿物岩石地球化学通报*, 2024, 43(2): 467–473.
- Liu X H, Meng Y M. There is a mystery in “germanium”, observe “germanium” to find the true meaning[J]. *Bulletin of Mineralogy, Petrology and Geochemistry*, 2024, 43(2): 467–473.
- [2] 赵君, 饶竹, 王鹏, 等. 黑龙江讷河市富锗土壤地球化学特征及影响因素浅析[J]. *岩矿测试*, 2022, 41(4): 642–651.
- Zhao J, Rao Z, Wang P, et al. Geochemical characteristics and influencing factors of germanium-enriched soils in Nehe City, Heilongjiang Province[J]. *Rock and Mineral Analysis*, 2022, 41(4): 642–651.
- [3] 叶霖, 韦晨, 胡宇思, 等. 锗的地球化学及资源储备展望[J]. *矿床地质*, 2019, 38(4): 711–728.
- Ye L, Wei C, Hu Y S, et al. Geochemistry of germanium and its resources reserves[J]. *Mineral Deposits*, 2019, 38(4): 711–728.
- [4] Cugeron A, Cenki-Tok B, Mu M, et al. Behavior of critical metals in metamorphosed Pb-Zn ore deposits: Example from the Pyrenean axial zone[J]. *Mineralium Deposita*, 2021, 56(4): 685–705.
- Cook N J, Ciobanu C L, Pring A, et al. Trace and minor elements in sphalerite: A LA-ICPMS study[J]. *Geochimica et Cosmochimica Acta*, 2009, 73(16): 4761–4791.
- [6] Lai X, Chen C H, Yang Y L, et al. Constraints on metallogenetic temperature and mineralization style from reflection color of sphalerite[J]. *Ore Geology Reviews*, 2023, 161: 105634.
- [7] 吴越, 孔志岗, 陈懋弘, 等. 扬子板块周缘MVT型铅锌矿床闪锌矿微量元素组成特征与指示意义: LA-ICP-MS研究[J]. *岩石学报*, 2019, 35(11): 3443–3460.
- Wu Y, Kong Z G, Chen M H, et al. Trace elements in sphalerites from the Mississippi Valley-type lead-zinc deposits around the margins of Yangtze Block and its geological implications: A LA-ICP-MS study[J]. *Acta Petrologica Sinica*, 2019, 35(11): 3443–3460.
- [8] 温汉捷, 周正兵, 朱传威, 等. 稀散金属超常富集的主要科学问题[J]. *岩石学报*, 2019, 35(11): 3271–3291.
- Wen H J, Zhou Z B, Zhu C W, et al. Critical scientific issues of super-enrichment of dispersed metals[J]. *Acta Petrologica Sinica*, 2019, 35(11): 3271–3291.
- [9] 周家喜, 杨德智, 余杰, 等. 贵州黄丝背斜地区实现大型共(伴)生锗矿床找矿突破[J]. *矿物学报*, 2020, 40(6): 772.
- Zhou J X, Yang D Z, Yu J, et al. A breakthrough in prospecting for large-scale germanium deposit in the Huangsi anticline area, Guizhou Province, China[J]. *Acta Mineralogica Sinica*, 2020, 40(6): 772.
- [10] 韩润生, 吴鹏, 王峰, 等. 论热液矿床深部大比例尺“四步式”找矿方法——以川滇黔接壤区毛坪富锗铅锌矿为例[J]. *大地构造与成矿学*, 2019, 43(2): 246–257.
- Han R S, Wu P, Wang F, et al. ‘Four Steps Type’ ore-prospecting method for deeply concealed hydrothermal ore deposits——A case study of the Maoping Zn-Pb-(Ag-Ge) deposit in southwestern China[J]. *Geotectonica et Metallogenesis*, 2019, 43(2): 246–257.
- [11] 韩润生, 吴鹏, 张艳, 等. 西南特提斯川滇黔成矿区富锗铅锌矿床成矿理论研究新进展[J]. *地质学报*, 2022, 96(2): 554–573.
- Han R S, Wu P, Zhang Y, et al. New research progress in metallogenetic theory for rich Zn-Pb-(Ag-Ge) deposits in the Sichuan—Yunnan—Guizhou Triangle (SYGT) area, southwestern Tethys[J]. *Acta Geologica Sinica*, 2022, 96(2): 554–573.
- [12] 郑绪忠. 四川乌斯河铅锌矿床地质特征及矿床成因[D]. 西安: 长安大学, 2012.
- Zheng X Z. Geological features and genesis of Wusihe Pb-Zn deposit, Sichuan[D]. Xi'an: Chang'an University, 2012.
- [13] Xiong S F, Gong Y J, Jiang S Y, et al. Ore genesis of the Wusihe carbonate-hosted Zn-Pb deposit in the Dadu River Valley district, Yangtze Block, SW China: Evidence from ore geology, S-Pb isotopes, and sphalerite Rb-Sr dating[J]. *Mineralium Deposita*, 2018, 53(7): 967–979.
- [14] 韦晨, 叶霖, 李珍立, 等. 四川乌斯河铅锌矿床成矿物质来源及矿床成因: 来自原位S-Pb同位素证据[J].

- 岩石学报, 2020, 36(12): 3783–3796.
- Wei C, Ye L, Li Z L, et al. Metal sources and ore genesis of the Wusihe Pb-Zn deposit in Sichuan, China: New evidence from *in-situ* S and Pb isotopes[J]. *Acta Petrologica Sinica*, 2020, 36(12): 3783–3796.
- [15] 熊索菲, 姚书振, 宫勇军, 等. 四川乌斯河铅锌矿床成矿流体特征及 TSR 作用初探[J]. 地球科学, 2016, 41(1): 105–120.
- Xiong S F, Yao S C, Gong Y J, et al. Ore-forming fluid and thermochemical sulfate reduction in the Wusihe lead-zinc deposit, Sichuan Province, China[J]. *Earth Science*, 2016, 41(1): 105–120.
- [16] 康许浩. 乌斯河铅锌矿床矿物成分特征[J]. 四川有色金属, 2022(1): 10–12.
- Kang X H. The mineral composition characteristics of Wusihe Pb-Zn deposit[J]. *Sichuan Nonferrous Metals*, 2022(1): 10–12.
- [17] 赵文皓, 陈翠华, 康许浩, 等. 四川乌斯河铅锌矿床闪锌矿微量元素特征及其指示意义[J]. 矿物岩石, 2024, 44(2): 62–73.
- Zhao W H, Chen C H, Kang X H, et al. Characteristics of trace elements in sphalerite and its indicative significance in Wusihe deposit, Sichuan Province[J]. *Mineralogy and Petrology*, 2024, 44(2): 62–73.
- [18] 罗开, 周家喜, 徐畅, 等. 四川乌斯河大型锗铅锌矿床锗超常富集特征及其地质意义[J]. 岩石学报, 2021, 37(9): 2761–2777.
- Luo K, Zhou J X, Xu C, et al. The characteristics of the extraordinary germanium enrichment in the Wusihe large-scale Ge-Pb-Zn deposit, Sichuan Province, China and its geological significance[J]. *Acta Petrologica Sinica*, 2021, 37(9): 2761–2777.
- [19] 竺成林, 王华建, 叶云涛, 等. 基于原位多元素成像分析龙马溪组笔石成因及地质意义[J]. 岩矿测试, 2019, 38(3): 245–259.
- Zhu C L, Wang J H, Ye Y T, et al. The formation mechanism and geological significance of graptolite from the Longmaxi Formation: Constraints from *in situ* multi-element imaging analysis[J]. *Rock and Mineral Analysis*, 2019, 38(3): 245–259.
- [20] 范晨子, 孙冬阳, 赵令浩, 等. 激光剥蚀电感耦合等离子体质谱法微区原位定量分析锂铍矿物化学成分[J]. 岩矿测试, 2024, 43(1): 87–100.
- Fan C Z, Sun D Y, Zhao L H, et al. *In situ* quantitative analysis of chemical composition of lithium and beryllium minerals by laser ablation inductively coupled plasma-mass spectrometry[J]. *Rock and Mineral Analysis*, 2024, 43(1): 87–100.
- [21] 员媛娇, 范成龙, 吕喜平, 等. 电子探针和 LA-ICP-MS 技术研究内蒙古浩尧尔忽洞金矿床毒砂矿物学特征[J]. 岩矿测试, 2022, 41(2): 211–225.
- Yuan Y J, Fan C L, Lyu X P, et al. Application of EPMA and LA-ICP-MS to study mineralogy of arsenopyrite from the Haoyaerhudong gold deposit, Inner Mongolia, China[J]. *Rock and Mineral Analysis*, 2022, 41(2): 211–225.
- [22] Hardy A C. Handbook of colorimetry[J]. *Massachusetts Institute of Technology*, 1936, 85: 545–546.
- [23] Liu Y, Hu Z, Gao S, et al. *In situ* analysis of major and trace elements of anhydrous minerals by LA-ICP-MS without applying an internal standard[J]. *Chemical Geology*, 2008, 257(1–2): 34–43.
- [24] Wei C, Ye L, Hu Y S, et al. Distribution and occurrence of Ge and related trace elements in sphalerite from the Lehong carbonate-hosted Zn-Pb deposit northeastern Yunnan, China: Insights from SEM and LA-ICP-MS studies[J]. *Ore Geology Reviews*, 2019, 115: 103175.
- [25] Liu G X, Yuan F, Deng Y F, et al. Critical metal enrichment in carbonate-hosted Pb-Zn systems: Insight from the chemistry of sphalerite within the Hehuashan Pb-Zn deposit, middle-lower Yangtze River metallogenic belt, East China[J]. *Ore Geology Reviews*, 2022, 151: 105209.
- [26] 吉晓佳. 会泽铅锌矿闪锌矿中锗的赋存状态研究和元素替代机制探讨[D]. 北京: 中国地质大学(北京), 2019.
- Ji X J. Occurrence of germanium and element alternative mechanism in sphalerite from Huize Pb-Zn deposit[D]. Beijing: China University of Geosciences (Beijing), 2019: 1–39.

- [27] 李会来,李凡,张鼎文,等.低温剥蚀LA-ICP-MS准确测定硫化物矿物多元素分析研究[J].*岩矿测试*,2023,42(5): 970–982.
- Li H L, Li F, Zhang D W, et al. Multi-element accurate analysis of sulfide minerals by low-temperature ablation LA-ICP-MS[J]. *Rock and Mineral Analysis*, 2023, 42(5): 970–982.
- [28] 张效瑞,吴柏林,雷安贵,等.砂岩型铀矿成矿期与非成矿期黄铁矿的微区原位Pb同位素识别特征[J].*岩矿测试*,2022,41(5): 717–732.
- Zhang X R, Wu B L, Lei A G, et al. *In-situ* micro-scale Pb isotope identification characteristics of metallogenic and non-metallogenic pyrites in sandstone-type uranium deposits[J]. *Rock and Mineral Analysis*, 2022, 41(5): 717–732.
- [29] 代堰锫,余心起,吴淦国,等.北武夷蔡家坪铅锌矿床硫化物特征、矿床成因类型及成矿时代[J].地学前缘,2011,18(2): 321–338.
- Dai Y P, Yu X Q, Wu G G, et al. Characteristics of sulfide minerals, genetic type and metallogenic epoch of the Caijiaping lead-zinc deposit North Wuyi area, Jiangxi Province[J]. *Earth Science Frontiers*, 2011, 18(2): 321–338.
- [30] Frenzel M, Hirsch T, Gutzmer J. Gallium, germanium, indium, and other trace and minor elements in sphalerite as a function of deposit type—A meta-analysis[J]. *Ore Geology Reviews*, 2016, 76: 52–78.
- [31] Cave B, Lilly R, Hong W. The effect of co-crystallising sulphides and precipitation mechanisms on sphalerite geochemistry: A case study from the Hilton Zn-Pb (Ag) deposit, Australia[J]. *Minerals*, 2020, 9: 1–22.
- [32] Oyebamiji A, Hu R Z, Zhao C H, et al. Origin of the Triassic Qilinchang Pb-Zn deposit in the western Yangtze Block, SW China: Insights from *in-situ* trace elemental compositions of base metal sulphides[J]. *Journal of Asian Earth Sciences*, 2020, 192: 1–21.
- [33] Yang Q Z, Xiao J, Ulrich T, et al. Trace element compositions of sulfides from Pb-Zn deposits in the northeast Yunnan and northwest Guizhou Provinces, SW China: Insights from LA-ICP-MS analyses of sphalerite and pyrite[J]. *Ore Geology Reviews*, 2022, 141: 1–22.
- [34] Li G M, Zhao Z X, Wei J H, et al. Trace element compositions of galena in an MVT deposit from the Sichuan—Yunnan—Guizhou metallogenic province, SW China: Constraints from LA-ICP-MS spot analysis and elemental mapping[J]. *Ore Geology Reviews*, 2022, 150: 1–20.